EARTHQUAKE ENGINEERING AND STRUCTURAL DYNAMICS, VOL. 7, 509-527 (1979)

GENERATION OF ARTIFICIAL STRONG MOTION ACCELEROGRAMS

H. L. WONG AND M. D. TRIFUNAC

Department of Civil Engineering, University of Southern California, California, U.S.A.

SUMMARY

A method for generating synthetic strong motion accelerograms for use in engineering design is presented. This method utilizes the model proposed by Trifunac in 1971[27] in conjunction with the recent empirical scaling functions for characterization of amplitudes and duration of strong shaking in terms of (i) earthquake magnitude, M, and epicentral distance, R, or (ii) Modified Mercalli Intensity (MMI) at the recording station. The method also enables one to consider the desired levels of confidence that the synthetic motion will not be exceeded, direction of ground motion (horizontal or vertical) and the dispersive properties of geologic environment beneath and surrounding the station. The principal features of this approach are that the resulting accelerograms have non-stationary frequency and amplitude characteristics which are in full agreement with known principles of wave propagation through a stratified medium, and that the Fourier amplitudes and the frequency-dependent duration are scaled in accordance with known trends as in recorded accelerograms.

INTRODUCTION

After 45 years of strong motion recording programs in the western United States, less than 200 significant strong motion accelerograms have been recorded, processed and analysed.[16] While these data do represent a unique and invaluable collection for studies of strong earthquake ground motion, they do not cover all different recording conditions to represent a complete observational basis for use in engineering design. Thus, for certain engineering applications it is necessary to estimate future shaking at a site, often outside the range of parameters for which recorded data are now available. Furthermore, considerable variability in the characteristics of recorded motion even under similar conditions may require a characterization of future shaking in terms of an ensemble of accelerograms rather than one or two 'typical' records. This and related requirements have created a need for the development of techniques for generation of artificial time histories that simulate realistic ground shaking with different degrees of detail and from different viewpoints. In this paper, we present a refinement of the method presented by Trifunac.[27]

Apparent overall irregularity of early recorded accelerograms[12] and the limited number of records in the 1950's have led some investigators to explore the possibility of modelling strong ground shaking by means of random time functions of simple but known properties. Thus, Housner,[13] for example, assumed that an accelerogram could be modelled by a series of one-cycle sine-wave pulses. Others used a series of pulses distributed randomly in time.[5,7,15,22,23] On the basis of such artificial time functions of known statistical properties, it became possible to study the response of hysteretic structures[14] and to design for the effects of seismic forces on the basis of probability methods.[9,19,25]

With the increasing number of recorded accelerograms in the 1950's and early 1960's, it became clear[4] that the non-stationarity of ground motion can influence structural response significantly. This prompted the development of a number of non-stationary random time series methods for the construction of artificial accelerograms.[2,3,6,8,10,17,18,24] The non-stationarity in these models was achieved typically by (a) multiplying stationary random time series by a non-stationary envelope function, by (b) changing the frequency content of artificial accelerograms as a function of time, and by (c) superimposing simple earthquake sources with some phase delay in time[20] to represent propagation of a simple earthquake source[11] by means of radiated P- and S-waves only.

0098-8847/79/0607-0509$01.00

Received 30 November 1978
Revised 27 March 1979

Recent observational studies of strong ground motion have shown that a typical strong motion record consists of near-field, intermediate field, body waves and surface waves contributing different amounts to the total result, depending on the earthquake source mechanism and on the wave path.[26, 29–31] Empirical studies of spectral characteristics[32, 33] and of the frequency-dependent duration[34, 35] have further shown the dependence on the geologic environment of the recording station. Consequently, realistic artificial accelerograms should have non-stationary frequency, amplitude and duration characteristics that agree with the trends which are now known to be present in the recorded accelerograms.

The purpose of this paper is to present an engineering method for generating artificial strong motion accelerograms which

(i) have Fourier *amplitude* spectra consistent with spectra computed from recorded accelerograms in conditions characterized by (a) magnitude, M, and source-to-station distance, R[32] or (b) Modified Mercalli Intensity (MMI) at the site;[33]

(ii) have duration of strong shaking which is consistent with observations and with empirical scaling of the duration in terms of M and R[34] or MMI;[35] and

(iii) have overall transient time characteristics with wave arrivals consistent with dispersive properties of the wave guide beneath the recording station.[26, 27]

Artificial accelerograms with proper dispersive characteristics and realistic wave arrival times cannot be derived from Fourier *amplitude* spectra only.[32, 33] This is because, so far, a method for empirical scaling of Fourier *phase* spectra in terms of geologic characteristics of a site has not been developed. This seems as difficult as correlating the complete acceleration time function with the local geology data. To avoid this difficult task, in this paper we show how, by means of a scaling factor α, the assumed spectral amplitudes at any given frequency ω, and containing all information on the dispersion, can be changed to agree with spectral amplitudes consistent with observations and with the above three requirements.

THEORETICAL BASIS

Most empirical scaling procedures neglect the phase of the Fourier spectrum of acceleration since a regression analysis involving the phase of the Fourier transform is equivalent in difficulty to correlating the time histories themselves. Instead, just the modulus of the Fourier transform is typically correlated with pertinent scaling parameters. These correlations may take many different forms depending on which parameters are used to characterize strong ground motion.[32, 33]

To describe the method presented in this report we begin by considering a group of harmonic waves having a Fourier transform of the form

$$F_1(\omega) = \begin{cases} c_1 \exp\left[-\mathrm{i}(\omega-\omega_n)\, t_1^* + i\phi_1\right], & \text{for } \omega_n - \Delta\omega \leqslant \omega \leqslant \omega_n + \Delta\omega \\ c_1 \exp\left[-\mathrm{i}(\omega+\omega_n)\, t_1^* - \mathrm{i}\phi_1\right], & \text{for } -\omega_n - \Delta\omega \leqslant \omega \leqslant -\omega_n + \Delta\omega \\ 0, & \text{otherwise} \end{cases} \tag{1}$$

$|F_1(\omega)|$ has a constant amplitude c_1 and its wave form in the time domain is

$$f_1(t) = \frac{1}{2\omega}\int_{-\infty}^{\infty} F_1(\omega)\exp(\mathrm{i}\omega t)\,\mathrm{d}\omega = Q_1(t)\cos(\omega_n t + \phi_1) \tag{2}$$

in which $Q_1(t)$ is an envelope function

$$Q_1(t) = \frac{2c_1}{\pi}\,\frac{\sin\Delta\omega(t-t_1^*)}{t-t_1^*} \tag{3}$$

The function $Q_1(t)$ has its maximum at $t = t_1^*$, and it decreases as $|t-t_1^*|$ increases. The quantity t_1^* can be viewed here as the arrival time for the wave group $f_1(t)$.

Consider now a second group of waves

$$f_2(t) = \frac{2c_2}{\pi}\,\frac{\sin\Delta\omega(t-t_2^*)}{t-t_2^*}\cos(\omega_n t + \phi_2) \tag{4}$$

It has a constant Fourier amplitude $|F_2(\omega)|$ of c_2 over the same frequency band as $f_1(t)$, i.e.

$$F_2(\omega) = \begin{cases} c_2 \exp[-i(\omega-\omega_n)t_2^* + i\phi_2], & \text{for } \omega_n - \Delta\omega \leqslant \omega \leqslant \omega_n + \Delta\omega \\ c_2 \exp[-i(\omega+\omega_n)t_2^* - i\phi_2], & \text{for } -\omega_n - \Delta\omega \leqslant \omega \leqslant -\omega_n + \Delta\omega \\ 0, & \text{otherwise} \end{cases} \tag{5}$$

When these two groups of waves are superimposed as

$$g(t) = f_1(t) + f_2(t) \tag{6}$$

the Fourier amplitude of $g(t)$ is no longer constant, and becomes

$$|G(\omega)| = |F_1(\omega) + F_2(\omega)| = \sqrt{\{c_1^2 + c_2^2 + 2c_1 c_2 \cos[(\omega-\omega_n)(t_1^* - t_2^*) + (\phi_2 - \phi_1)]\}} \tag{7}$$

a function of ω over the interval, $\omega_n - \Delta\omega \leqslant |\omega| \leqslant \omega_n + \Delta\omega$.

The oscillatory characteristics of $|G(\omega)|$ about its mean are such that the amplitude is controlled by the difference in amplitudes of c_1 and c_2 and the rate of oscillation is controlled by the difference in arrival times, $(t_1^* - t_2^*)$. Therefore, the irregularities of a typical Fourier amplitude spectrum can be thought of as being the interferences caused by many wave groups arriving at the site with different amplitudes and at different times.

To reconstruct an accelerogram from the Fourier amplitude spectrum, one must have the following information: (i) the arrival times and (ii) the relative amplitudes of different waves. For the latter task, only relative amplitudes are needed because the absolute amplitude of the combined time history is given by the Fourier amplitude spectrum of the complete artificial accelerogram.

GENERATION OF SYNTHETIC ACCELEROGRAMS

Wave propagation studies have shown that in an inhomogeneous medium the surface waves and body waves travel at different velocities. Furthermore, in layered media surface waves travel in a dispersive manner, their velocities depending on the material properties of the medium, the frequency of wave motion and the geometrical configuration of the layers. The group velocities for a particular site can be estimated either by processing of previous records using techniques in observational seismology or by theoretical calculations. At present, most theoretical models are based on horizontal parallel layers. An example is shown in Figure 1, in which an approximate profile for the El Centro, California site is used. Although the assumption of horizontal layers is a restrictive one, it is advantageous to use theoretically calculated dispersion curves for the generation of arrival times of different phases because experimentally derived results may not be available for all sites and it is also difficult to obtain them for high frequencies.

Once the dispersion curves have been computed, the arrival times of the mth mode at ω_n can be written as

$$t_{nm}^* = R/U_m(\omega_n) \tag{8}$$

where R is the distance from the source to the station and $U_m(\omega_n)$ is the group velocity of the mth mode at the frequency band centred at ω_n.

One can select the frequency bands narrow enough, i.e. $\Delta\omega_n$ is small enough, so that $U_m(\omega)$ is approximately constant throughout, $\omega_n - \Delta\omega_n \leqslant \omega \leqslant \omega_n + \Delta\omega_n$. Then the contribution to the total accelerogram from this particular frequency band can be expressed as

$$h_n(t) = \sum_{m=1}^{M} \alpha_n A_{nm} \frac{\sin \Delta\omega_n (t - t_{nm}^*)}{t - t_{nm}^*} \cos(\omega_n t + \phi_n) \tag{9}$$

where M is the total number of surface wave modes, ϕ_n is a phase introduced to include random effects of source dislocation and other miscellaneous effects along the propagation path, ω_n is the centre frequency, and t_{nm}^* is the arrival time of the mth mode given by equation (8). The amplitude of each mode is currently defined as $\alpha_n A_{nm}$, A_{nm} being the relative amplitudes of different surface wave modes and α_n is a scale factor to be used for determining the final amplitude through a specified overall Fourier amplitude spectrum $\mathrm{FS}(\omega_n)$.

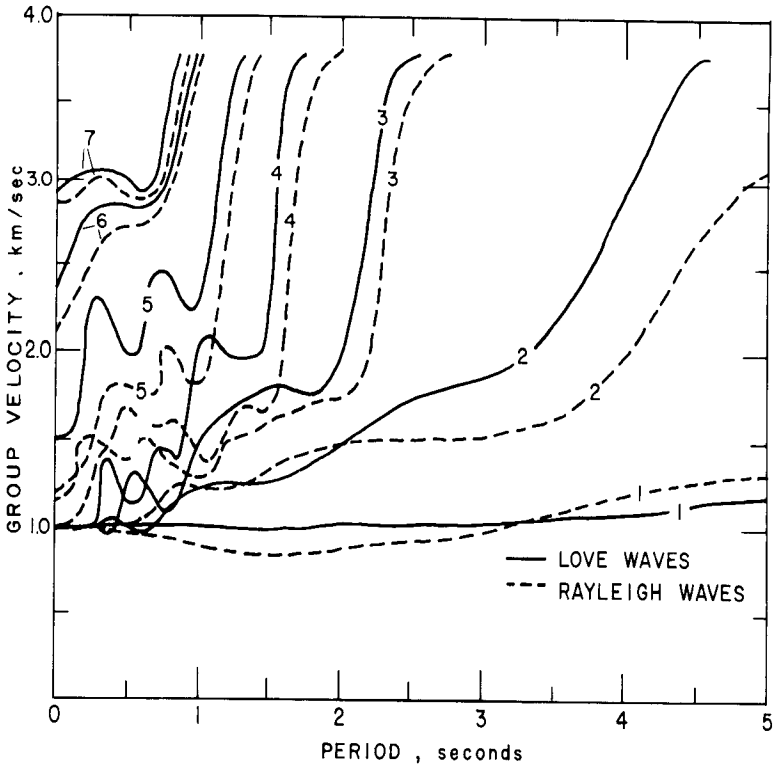

Figure 1

With all the different waves arriving at different instances, the Fourier amplitude of $h_n(t)$,

$$|H_n(\omega)| = \begin{cases} \left| \sum_{m=1}^{M} \frac{\pi}{2} \alpha_n A_{nm} \exp\left[-i(\omega-\omega_n) t^*_{nm} - \phi_n)\right] \right|, & \text{for } \omega_n - \Delta\omega \leqslant |\omega| \leqslant \omega_n + \Delta\omega_n \\ 0, & \text{otherwise} \end{cases} \tag{10}$$

is an irregular function over a narrow band of $2\Delta\omega$. We match its mean amplitude so that

$$\int_{\omega_n-\Delta\omega_n}^{\omega_n+\Delta\omega_n} |H_n(\omega)|\, d\omega \Big/ 2\Delta\omega_n = \mathrm{FS}(\omega_n) \tag{11}$$

Thus, by substituting equation (10) into (11), one can solve for the scale factor α_n as

$$\alpha_n = 2\Delta\omega_n \mathrm{FS}(\omega_n) \Big/ \frac{\pi}{2} \int_{\omega_n-\Delta\omega_n}^{\omega_n+\Delta\omega_n} \left| \sum_{m=1}^{M} A_{nm} \exp\left[-i((\omega-\omega_n) t^*_{nm} - \phi_n)\right] \right| d\omega \tag{12}$$

A similar procedure can be applied to other frequency bands within the frequencies of interest. For a Fourier analysis divided into N non-overlapping bands, the total accelerogram can be expressed as

$$a(t) = \sum_{m=1}^{N} \alpha_n \sum_{m=1}^{M} A_{nm} \frac{\sin \Delta\omega_n (t - t^*_{nm})}{t - t^*_{nm}} \cos(\omega_n t + \phi_n) \tag{13}$$

As pointed out by Trifunac[27] body P- and S-waves could be modelled for purposes of generating artificial accelerograms for use in engineering response calculations in two different ways. One approach would consist of adding two bursts of energy to the surface wave motions modelled by (9). Another simpler approach adopted in this paper is to merely add 'higher order modes' to the dispersion curves of surface waves and to select A_{nm} so that contributions of these modes 'represent' P- and S-wave arrivals. Surface wave modes 6 and 7 in Figure 1 have been chosen in this manner for examples shown in this work.

Calculation of A_{nm} and ϕ_n

Depending upon the faulting mechanism and the wave paths to the site, various amplitudes of body and surface waves will be excited. Some methods have been developed in seismology for the partitioning of energy radiated into these contributions, but for strong motion and for near field shaking, scaling of spectral

amplitudes based on the empirical scaling laws derived from recorded accelerograms may be preferable. For the accelerograms presented in this paper, A_{nm} was chosen to be as proposed by Trifunac.[27]

The values of A_{nm} as a function of frequency have been defined as

$$A_{nm}(\omega_n) = A_1(m)\,A_2(\omega_n) \tag{14}$$

where

$$A_1(m) = \left|\exp\left[-(m-m_0)^2/2C_0^2\right] + C_R\,X_{Rm}\right|$$

and

$$A_2(\omega_n) = \left|B_0 \exp\left[-(\omega_n-\omega_P)^2/2\omega_B^2\right] + B_R\,X_{Rn}\right|.$$

X_{Rm} and X_{Rn} are random numbers between -1 and 1, the other constants are defined in Table I. The phase ϕ_n is assumed to be random between $-\pi$ and π.

Table I

m	C_0	m_0	C_R	B_0	ω_P	ω_B	B_R
1	3	5	0·2	1·5	10	5	0·1
2	3	5	0·2	1·5	10	5	0·1
3	3	5	0·2	1·5	10	5	0·1
4	3	5	0·2	2·0	25	15	0·1
5	3	5	0·2	2·0	25	15	0·1
6	3	6	0·2	3·0	30	10	0·3
7	3	7	0·2	1·5	30	5	0·25

The Fourier amplitude spectrum

Since the Fourier amplitude spectrum (Figure 2)[32,33] is the most direct quantity that can be used for defining the amplitudes of an accelerogram, it is useful to derive detailed knowledge on how it varies as a function of the simple earthquake scaling parameters.

For scaling in terms of the earthquake magnitude, the Fourier spectrum, FS, as a function of period T is

$$\log_{10} \mathrm{FS}(T) = M + \log_{10} A_0(R) - a(T)\,p_l - b(T)\,M - c(T) - d(T)\,s - e(T)\,v - f(T)\,M^2 - g(T)\,R. \tag{15}$$

In this relationship, M is the magnitude, R is the epicentral distance, $v = 0$ for horizontal components and $v = 1$ for vertical components, and $s = 0$ for the alluvium sites, $s = 2$ for a site on the sound basement rock with $s = 1$ for 'intermediate' geologic conditions. The terms $a(T), b(T), \ldots, g(T)$ are regression coefficients found independently at each period (T). Following Trifunac,[32] for magnitudes $M \leqslant M_{\min} = -b(T)/2f(T)$, the terms $-b(T)\,M - f(T)\,M^2$ are replaced by the constant $-b(T)\,M_{\min} - f(T)\,M_{\min}^2$, and for magnitudes $M \geqslant M_{\max} = [1-b(T)]/2f(T)$, the terms $M - b(T)\,M - f(T)\,M^2$ are replaced by the constant

$$M_{\max} - b(T)\,M_{\max} - f(T)\,M_{\max}^2.$$

The term $\log_{10} A_0(R)$ is the attenuation function given by Richter[21] for the local magnitude scale in southern California. To apply this method correctly to another region, the coefficients in equation (15), or a comparable equation, should be derived entirely from data of that region. However, in the absence of such data, a reasonable approximation is to replace the term $\log_{10} A_0(R)$ derived for southern California with one applicable to the region considered.

The term $a(T)\,p_l$ describes the way the data are distributed about the mean curve, where p_l is approximately the probability that FS(T) will not be exceeded for a given M, R, s and v. The values of $a(T)$–$g(T)$ for eleven periods are given in Table II(a) while the attenuation factor $\log_{10} A_0(R)$ is shown in Table II(b).

For the scaling in terms of the Modified Mercalli Intensity (MMI), the regression equation has the form[33]

$$\log_{10} \mathrm{FS}(T) = a(T)\,p_l + b(T)\,I_{MM} + c(T) + d(T)\,s + e(T)\,v \tag{16}$$

in which I_{MM} is the integer corresponding to the level of intensity at the site. Other parameters such as p_l, s and v are defined in the same manner as in equation (15). The numerical values of a, b, c, d and $e(T)$ are given in Table III.

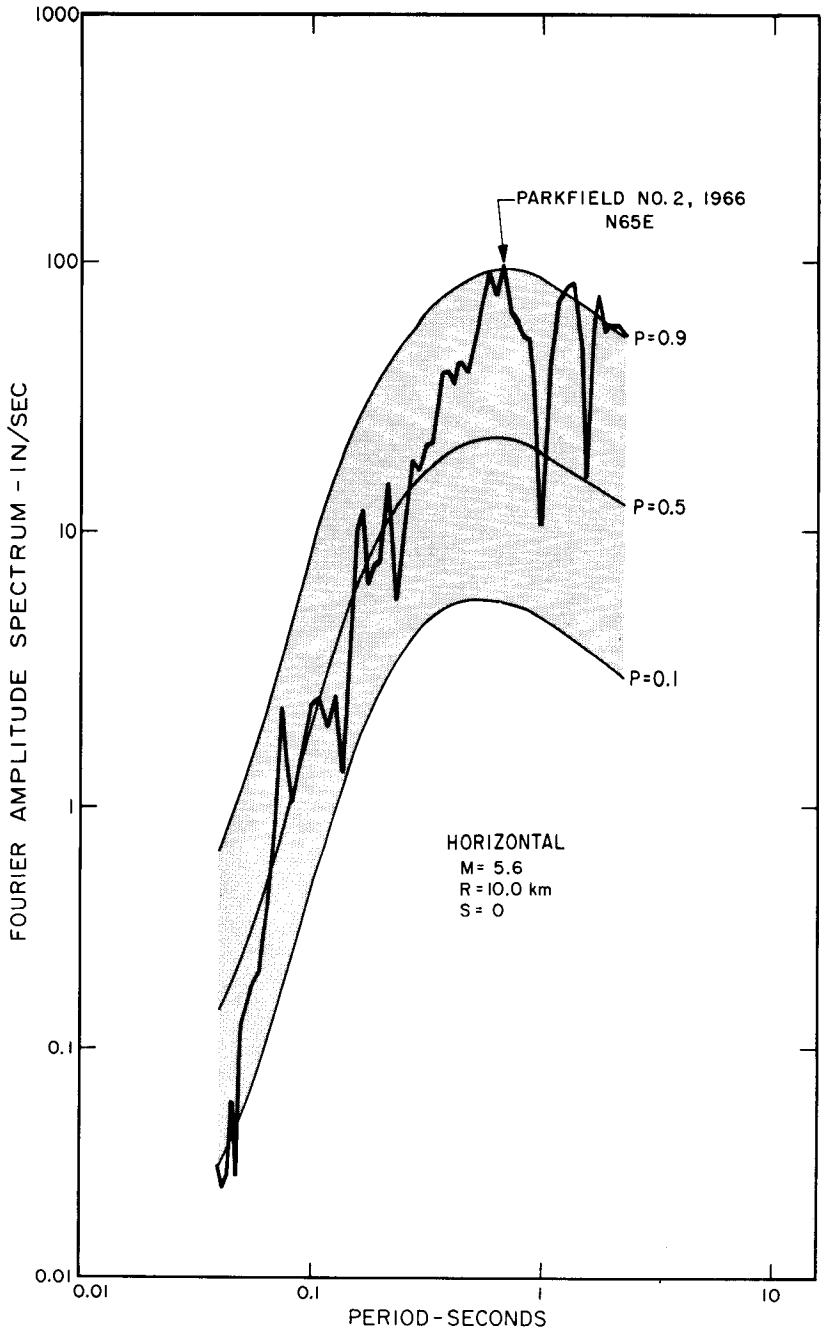

Figure 2

Equations (15) and (16) give Fourier amplitude spectra in terms of p_l which, for $0{\cdot}1 \leqslant p_l \leqslant 0{\cdot}9$, approximates the actual distribution, p_a, of spectral amplitudes about those two assumed models. It has been shown by Anderson and Trifunac[1] that p_a can be approximated by a Gaussian distribution function at all periods. They show that

$$p_a = \int_{-\infty}^{p_l} \frac{1}{\sigma(T)\sqrt{2\pi}} \exp\left[-\frac{1}{2}\left(\frac{\varepsilon-\mu(T)}{\sigma(T)}\right)^2\right] d\varepsilon$$

can be used to approximate p_a versus p_l and that this functional form is not rejected by either χ^2 or Kolmogorov–Smirnov tests of H_0 hypothesis. In this expression, $\mu(T)$ and $\sigma(T)$ represent the best values (in the sense of least squares) of mean and standard deviation and are determined from the data on FS amplitudes and for different periods T (see Tables II(a) and III).

Table II(a). Regression coefficients for Fourier amplitude parameters: M, R, s, v, p_t

$\log(T)$	$a(T)$	$b(T)$	$c(T)$	$d(T)$	$e(T)$	$10f(T)$	$1000g(T)$	$\sigma(T)$	$\mu(T)$
−1·398	−1·688	−1·086	7·615	−0·018	−0·098	1·320	−0·441	0·301	0·492
−1·150	−1·620	−1·380	7·892	−0·080	−0·026	1·527	−0·869	0·300	0·502
−0·903	−1·517	−1·418	7·344	−0·068	0·094	1·542	−1·052	0·299	0·500
−0·655	−1·445	−1·216	6·249	0·011	0·229	1·364	−0·940	0·289	0·488
−0·407	−1·460	−1·053	5·587	0·102	0·304	1·206	−0·709	0·281	0·479
−0·159	−1·514	−1·129	5·913	0·163	0·319	1·227	−0·610	0·280	0·479
0·088	−1·549	−1·499	7·328	0·189	0·309	1·469	−0·753	0·287	0·488
0·336	−1·570	−2·592	11·230	0·197	0·288	2·250	−1·033	0·301	0·511
0·584	−1·601	−4·042	16·381	0·200	0·281	3·300	−1·258	0·312	0·532
0·831	−1·630	−4·699	18·875	0·204	0·292	3·775	−1·352	0·302	0·522
1·079	−1·633	−4·872	19·715	0·203	0·297	3·900	−1·375	0·289	0·492

Table II(b). $\log_{10} A_0(R)$ versus epicentral distance R*

R (km)	$-\log_{10} A_0(R)$	R (km)	$-\log_{10} A_0(R)$	R (km)	$-\log_{10} A_0(R)$
0	1·400	140	3·230	370	4·336
5	1·500	150	3·279	380	4·376
10	1·605	160	3·328	390	4·414
15	1·716	170	3·378	400	4·451
20	1·833	180	3·429	410	4·485
25	1·955	190	3·480	420	4·518
30	2·078	200	3·530	430	4·549
35	2·199	210	3·581	440	4·579
40	2·314	220	3·631	450	4·607
45	2·421	230	3·680	460	4·634
50	2·517	240	3·729	470	4·660
55	2·603	250	3·779	480	4·685
60	2·679	260	3·828	490	4·709
65	2·746	270	3·877	500	4·732
70	2·805	280	3·926	510	4·755
80	2·920	290	3·975	520	4·776
85	2·958	300	4·024	530	4·797
90	2·989	310	4·072	540	4·817
95	3·020	320	4·119	550	4·835
100	3·044	330	4·164	560	4·853
110	3·089	340	4·209	570	4·869
120	3·135	350	4·253	580	4·885
130	3·182	360	4·295	590	4·900

* Only the first two digits may be assumed to be significant.

Unless a particular situation calls for a specified spectrum, the above two empirical scaling functions are capable of providing site-dependent Fourier amplitude spectra that are consistent with current observations.

Duration of strong shaking

For structural analyses that consider fatigue and non-linear response of structures, the excitation level alone is generally inadequate to characterize the response, and a description of the duration of strong shaking is also necessary. For this reason, in this work the duration is included as an important frequency-dependent quantity while generating a synthetic accelerogram.

The duration of strong shaking is closely related to the difference in arrival times of the fastest and the slowest waves. Thus, if a representative dispersion curve can be derived for the site, it is most likely that such an estimate of the duration will be in agreement with the empirical scaling relationships based on recorded accelerograms.

Table III. Regression coefficients for Fourier amplitude parameters: I_{MM}, s, v, p_l

log (T)	a(T)	b(T)	c(T)	d(T)	e(T)	σ(T)	μ(T)
−1·398	1·707	0·341	−4·295	0·159	0·011	0·321	0·476
−1·141	1·688	0·312	−3·467	0·222	0·025	0·326	0·496
−0·883	1·559	0·285	−2·523	0·178	−0·104	0·326	0·506
−0·626	1·387	0·272	−1·886	0·092	−0·264	0·315	0·501
−0·368	1·294	0·272	−1·626	0·023	−0·335	0·308	0·496
−0·111	1·316	0·286	−1·667	−0·016	−0·338	0·307	0·497
0·146	1·413	0·312	−1·937	−0·039	−0·277	0·314	0·508
0·404	1·516	0·320	−2·097	−0·079	−0·207	0·333	0·519
0·661	1·537	0·280	−1·947	−0·102	−0·234	0·342	0·522
0·919	1·485	0·216	−1·793	−0·063	−0·214	0·329	0·530
1·176	1·473	0·174	−1·983	−0·032	−0·014	0·318	0·541

Using the definition given by Trifunac and Brady,[36] the duration is estimated by the 'energy-like' quantity

$$I(t) = \int_0^t a^2(\tau)\,\mathrm{d}\tau \tag{17}$$

The duration T is defined so that $I(T)$ is 90 per cent of $I(\infty)$, i.e. T is taken to be the interval in time in which 90 per cent of the seismic energy is contributed to the motion at a point. Since the input vibrational energy represents an important parameter in measurements of fatigue, this definition of duration appears to be useful from a structural analysis point of view.

The duration has been correlated with different parameters describing characteristics of strong shaking in a manner similar to that used in scaling the Fourier amplitude spectra. In the work by Trifunac and Westermo,[34,35] the duration is analysed in six frequency bands, ranging from 0·125 Hz to 25 Hz as in Table IV.

Table IV

Band	Frequency range (Hz)	Centre frequency (Hz)
1	10–25	18
2	4–10	7
3	1·5–4	2·7
4	0·7–1·5	1·1
5	0·3–0·7	0·5
6	0·125–0·3	0·2

Table V. Regression coefficients, $D = as + bM + cR + d \pm \sigma$

Centre frequency	f_c = 18·0	f_c = 7·0	f_c = 2·7	f_c = 1·1	f_c = 0·5	f_c = 0·2
			Vertical acceleration			
a	−1·04	−1·23	−3·30	−5·83	−6·80	−4·45
b	0·34	1·38	2·12	0·51	−0·47	−1·09
c	0·12	0·08	0·08	0·08	0·06	0·08
d	3·43	−0·57	−0·95	16·16	29·57	30·62
σ	5·34	4·59	5·93	8·86	11·65	12·44
			Horizontal acceleration			
a	−1·66	−1·38	−2·75	−4·09	−4·82	−3·02
b	0·64	1·32	1·28	−0·36	1·68	−0·43
c	0·13	0·08	0·09	0·08	0·07	0·09
d	1·88	−0·77	1·42	16·41	11·82	22·00
σ	5·89	5·10	5·57	7·41	10·75	12·01

Table VI. Means, x, and standard deviations, σ, of the duration of strong ground motion for different site conditions and modified Mercalli intensities

Site intensity	Site class.		$f_c = 0{\cdot}2$			$f_c = 0{\cdot}5$			$f_c = 1{\cdot}1$			$f_c = 2{\cdot}7$			$f_c = 7{\cdot}0$			$f_c = 18{\cdot}0$		
			x	σ	n†	x	σ	n	x	σ	n	x	σ	n	x	σ	n	x	σ	n
III	0	Vert.	47·4		1	44·7		1	28·0		1	25·8		1	20·6		1	35·8		1
		Horiz.	42·5		2	35·6		2	24·6		2	17·6		2	13·4		2	25·6		2
	1	Vert.																		
		Horiz.																		
	2	Vert.																		
		Horiz.																		
IV	0	Vert.	43·2		1	41·5		1	54·2		1	49·4		1	34·8		1	53·8		1
		Horiz.	40·2		2	35·9		2	32·2		2	33·3		2	28·2		2	42·7		2
	1	Vert.	33·2		2	38·8		1	30·9		2	18·4		2	17·4		2	27·0		2
		Horiz.	34·9	9·71	4	35·9	3·68	2	26·0	4·40	4	18·2	2·06	4	12·2	4·23	4	19·5	3·03	4
	2	Vert.																		
		Horiz.																		
	0	Vert.	37·1	16·2	16	31·5	13·9	17	27·1	12·5	17	17·8	9·94	17	15·9	7·21	17	16·8	10·6	17
		Horiz.	30·9	13·8	32	29·6	13·5	34	21·9	10·2	34	16·5	9·20	34	15·1	8·23	34	18·4	12·0	34
V	1	Vert.	25·9	11·6	12	25·2	14·5	15	18·9	9·60	15	13·9	4·97	15	12·6	7·21	15	11·3	6·46	15
		Horiz.	25·0	12·4	24	22·6	13·1	30	17·9	8·98	30	12·3	6·14	30	11·9	7·19	30	12·1	6·98	30
	2	Vert.	15·1	8·70	2	14·9	7·70	2	15·2	6·80	2	10·9	1·90	2	7·10	0·50	2	8·60	0·80	2
		Horiz.	17·1	9·24	4	14·7	6·95	4	8·60	1·56	4	9·80	1·98	4	8·25	0·67	4	8·75	1·92	4
	0	Vert.	32·4	11·3	43	34·0	12·5	43	28·0	11·0	43	19·9	8·22	43	14·5	7·15	43	14·3	9·73	43
		Horiz.	29·3	12·6	86	29·4	12·7	86	23·8	9·26	86	18·2	8·30	86	13·4	7·13	86	15·8	10·6	86
VI	1	Vert.	35·4	13·4	15	34·5	13·1	16	21·1	9·20	16	12·3	4·55	16	9·42	3·68	16	11·0	6·94	16
		Horiz.	33·3	12·6	30	30·2	12·3	32	18·6	9·41	32	10·2	4·99	32	7·59	3·99	32	9·24	7·16	32
	2	Vert.	23·4	10·3	7	14·4	7·56	7	10·1	4·20	7	10·1	5·35	7	11·3	4·88	7	8·60	2·56	7
		Horiz.	22·3	9·88	14	14·9	7·48	14	8·69	5·22	14	9·10	4·83	14	9·87	3·59	14	7·87	3·61	14
	0	Vert.	24·7	11·3	48	25·5	8·34	49	20·1	6·28	49	14·4	5·58	49	11·3	5·14	49	11·1	4·49	49
		Horiz.	20·2	11·0	96	22·4	8·12	98	14·9	5·28	98	11·4	4·93	98	10·7	6·01	98	11·2	6·20	98
VII	1	Vert.	17·3	7·01	21	16·1	4·04	21	13·4	3·91	21	10·9	3·17	21	9·04	2·64	21	8·81	1·84	21
		Horiz.	11·4	4·00	42	14·9	5·20	42	10·2	2·90	42	8·12	2·35	42	7·80	2·65	42	8·88	3·14	42
	2	Vert.	14·2	4·58	5	11·6	5·14	5	10·1	3·05	5	7·16	2·68	5	5·72	2·98	5	6·16	3·37	5
		Horiz.	12·6	3·22	10	11·5	3·47	10	8·18	3·24	10	4·92	2·50	10	4·98	2·86	10	6·36	3·62	10
	0	Vert.	25·5	17·1	6	35·0	13·1	6	25·3	11·7	6	20·1	10·7	6	13·7	7·74	6	11·7	6·69	6
		Horiz.	25·6	12·9	12	28·5	12·9	12	18·6	8·25	12	15·8	9·41	12	14·0	7·62	12	13·5	8·25	12
VIII and IX	1	Vert.																		
		Horiz.																		
	2	Vert.																		
		Horiz.																		
	0	Vert.																		
		Horiz.																		
X	1	Vert.																		
		Horiz.																		
	2	Vert.	11·4		1	5·20		1	6·60		1	6·00		1	7·00		1	8·00		1
		Horiz.	10·4		2	6·90		2	5·70		2	6·30		2	7·10		2	6·20		2

† Number of data points.

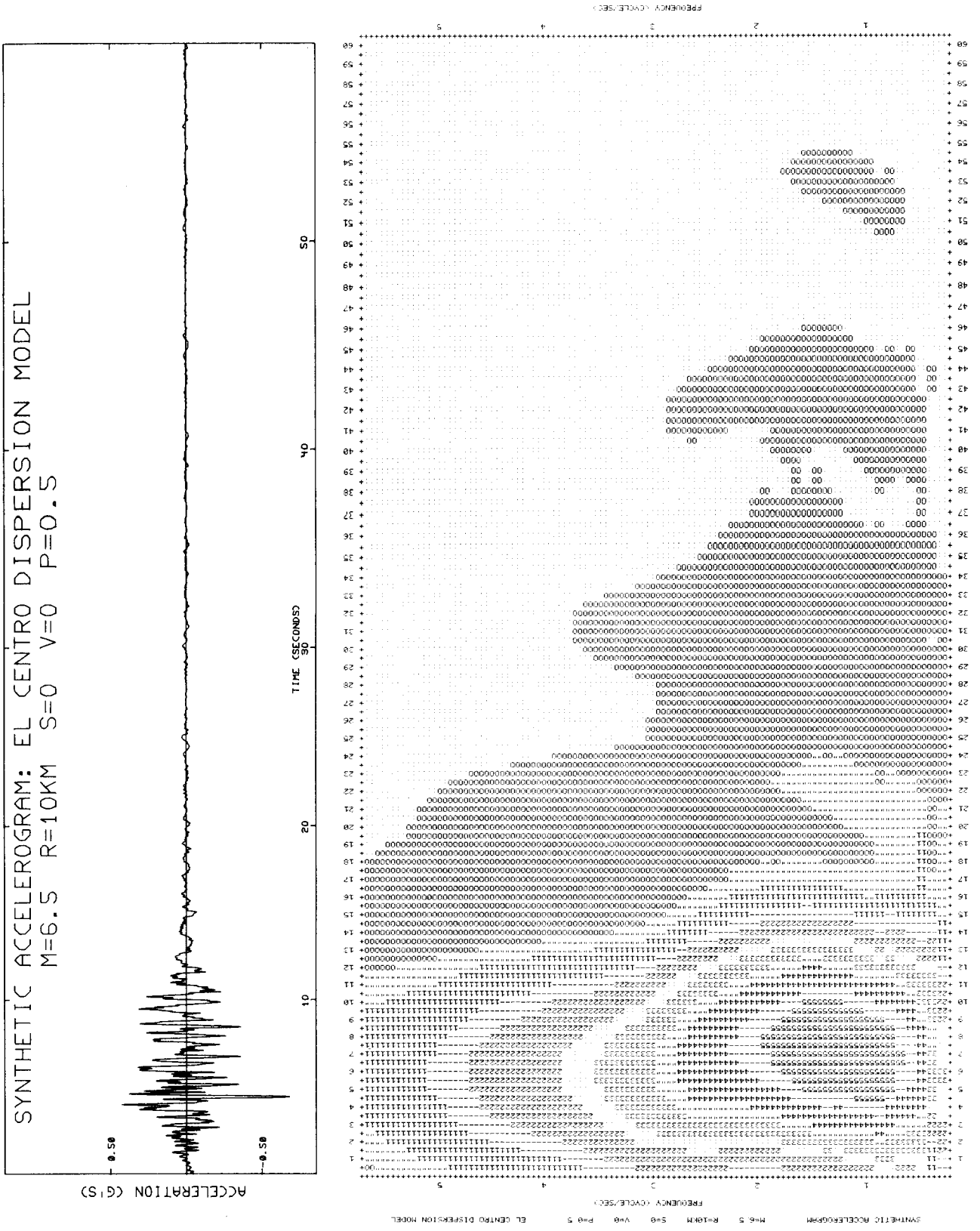
SYNTHETIC ACCELEROGRAM: EL CENTRO DISPERSION MODEL
M=6.5 R=10KM S=0 V=0 P=0.5
ACCELERATION (G'S)
0.50
-0.50
TIME (SECONDS)
10
20
30
40
50
FREQUENCY (CYCLE/SEC)
1
2
3
4
5
SYNTHETIC ACCELEROGRAM M=6.5 R=10KM S=0 V=0 P=0.5 EL CENTRO DISPERSION MODEL

Figure 3

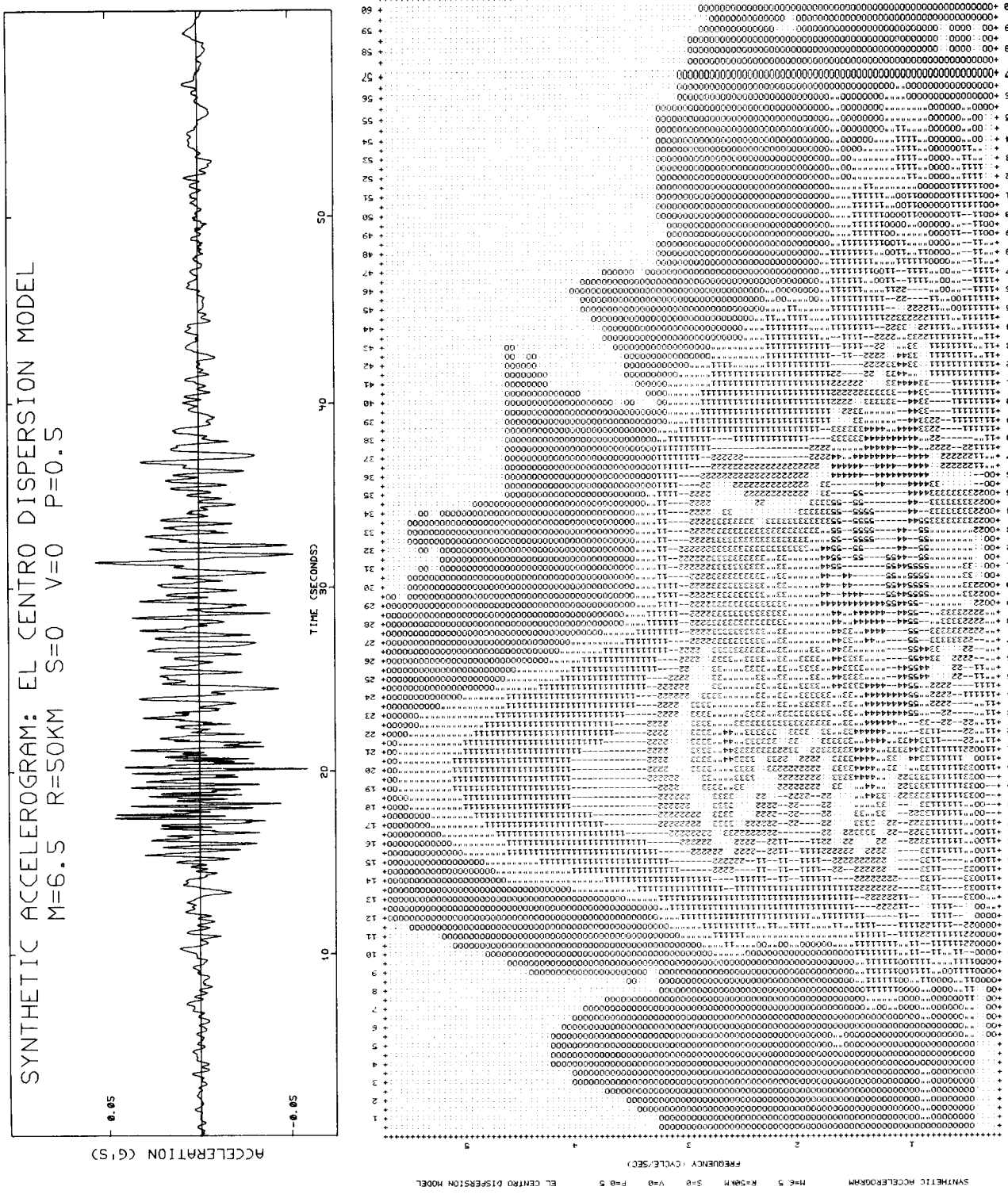
SYNTHETIC ACCELEROGRAM: EL CENTRO DISPERSION MODEL
M=6.5 R=50KM S=0 V=0 P=0.5
ACCELERATION (G'S)
TIME (SECONDS)
0.05
-0.05
10
20
30
40
50
FREQUENCY (CYCLE/SEC)
SYNTHETIC ACCELEROGRAM M=6.5 R=50KM S=0 V=0 P=0.5 EL CENTRO DISPERSION MODEL

Figure 4

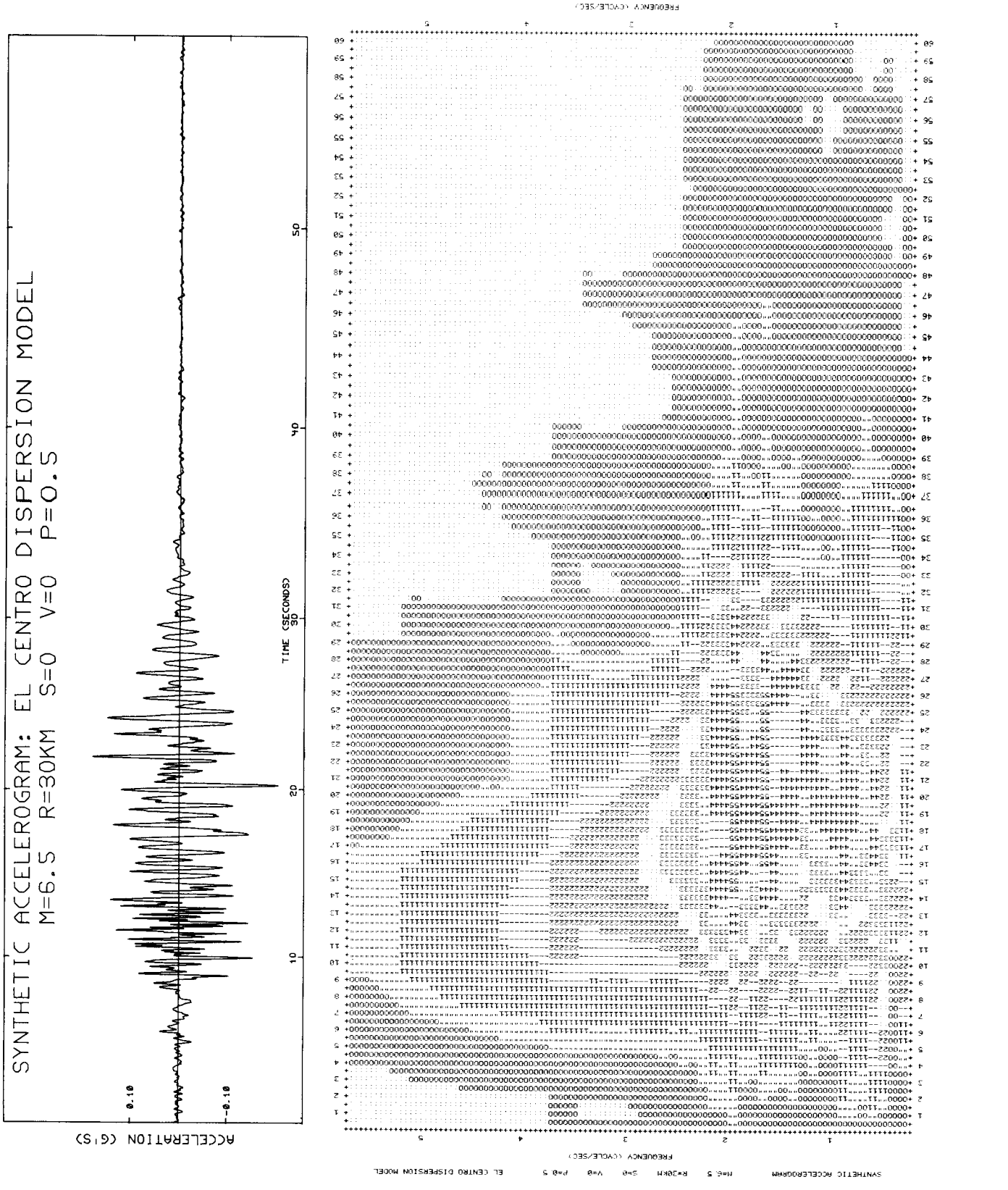
SYNTHETIC ACCELEROGRAM: EL CENTRO DISPERSION MODEL
M=6.5 R=30KM S=0 V=0 P=0.5
ACCELERATION (G'S)
TIME (SECONDS)
0.10
-0.10
10
20
30
40
50
FREQUENCY (CYCLE/SEC)
SYNTHETIC ACCELEROGRAM M=6.5 R=30KM S=0 V=0 P=0.5 EL CENTRO DISPERSION MODEL

Figure 5

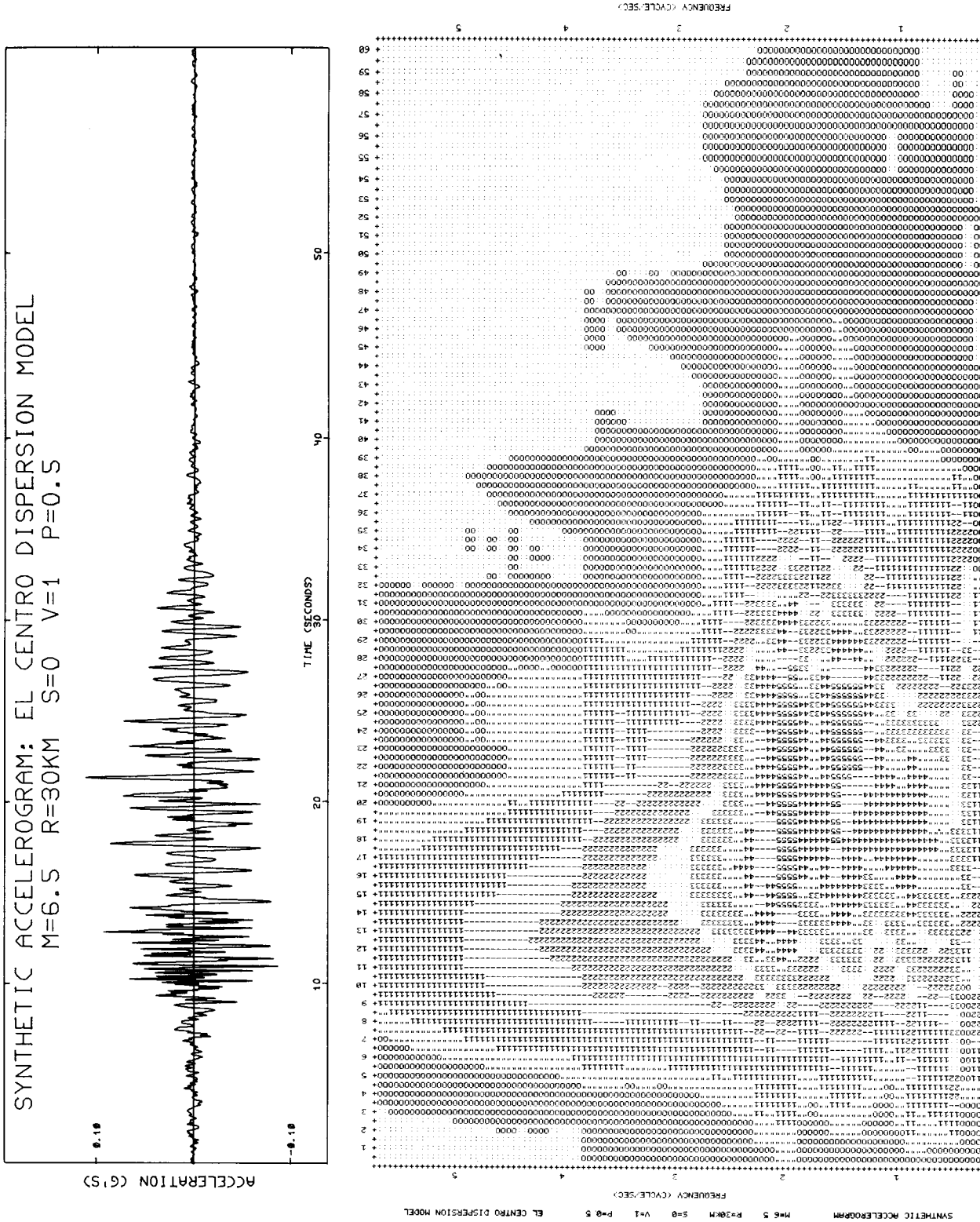
SYNTHETIC ACCELEROGRAM: EL CENTRO DISPERSION MODEL
M=6.5 R=30KM S=0 V=1 P=0.5
ACCELERATION (G'S)
TIME (SECONDS)
FREQUENCY (CYCLE/SEC)

Figure 6

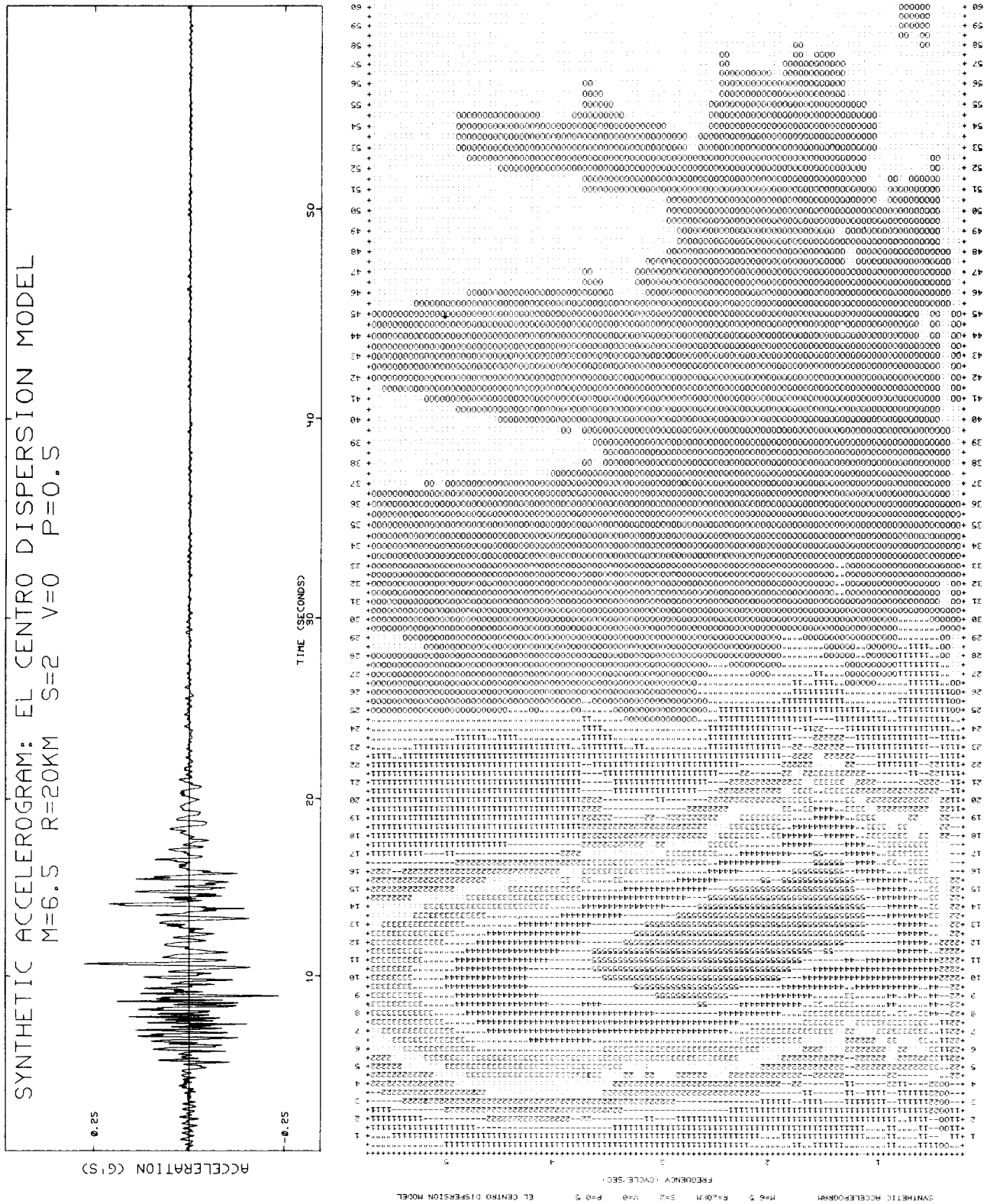
SYNTHETIC ACCELEROGRAM: EL CENTRO DISPERSION MODEL
M=6.5 R=20KM S=2 V=0 P=0.5
ACCELERATION (G'S)
TIME (SECONDS)
0.25
-0.25
10
20
30
40
50
FREQUENCY (CYCLE/SEC)
SYNTHETIC ACCELEROGRAM M=6.5 R=20KM S=2 V=0 P=0.5 EL CENTRO DISPERSION MODEL

Figure 7

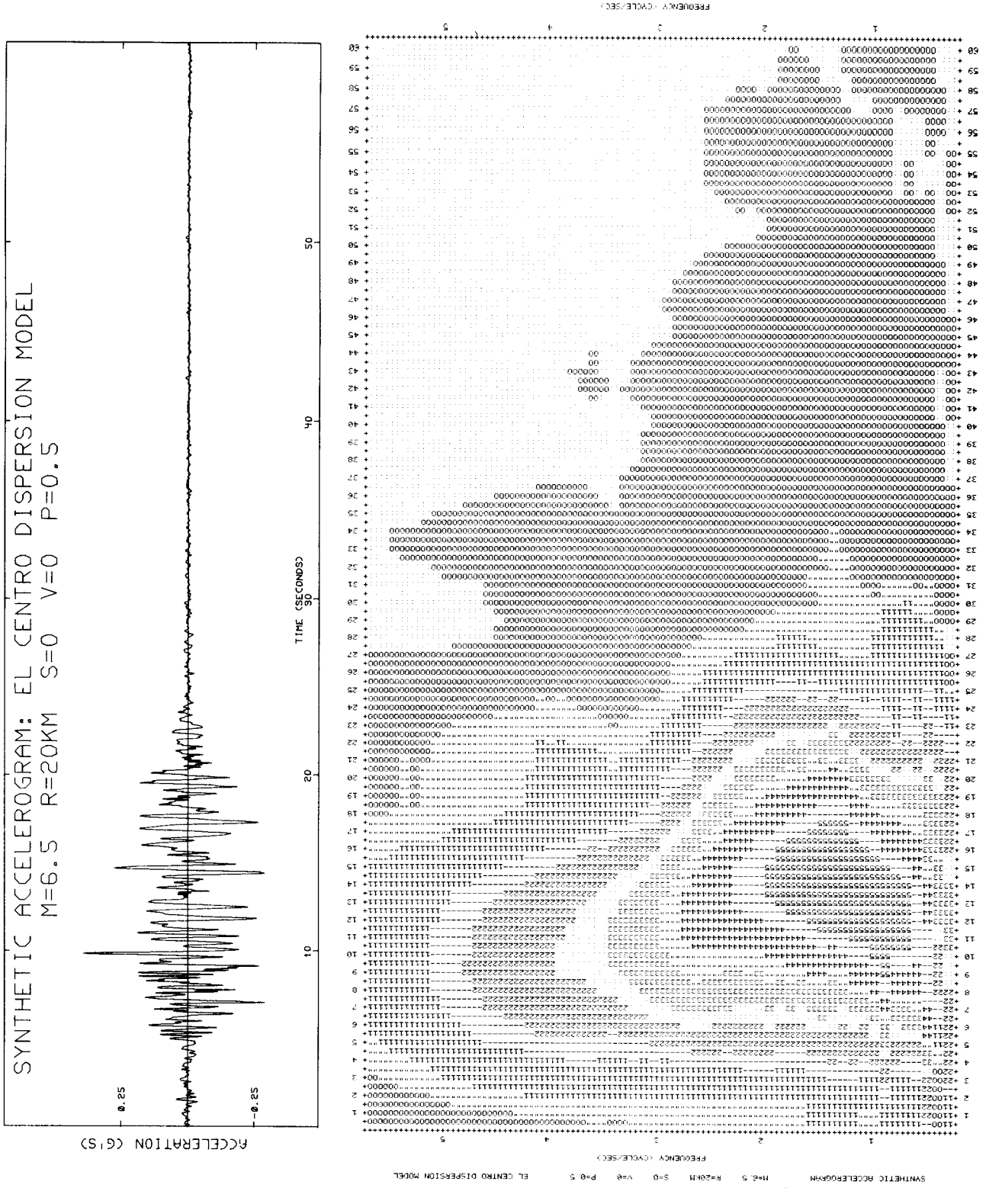
SYNTHETIC ACCELEROGRAM: EL CENTRO DISPERSION MODEL
M=6.5 R=20KM S=0 V=0 P=0.5
ACCELERATION (G'S)
0.25
-0.25
TIME (SECONDS)
10
20
30
40
50
FREQUENCY (CYCLE/SEC)
1
2
3
4
5

Figure 8

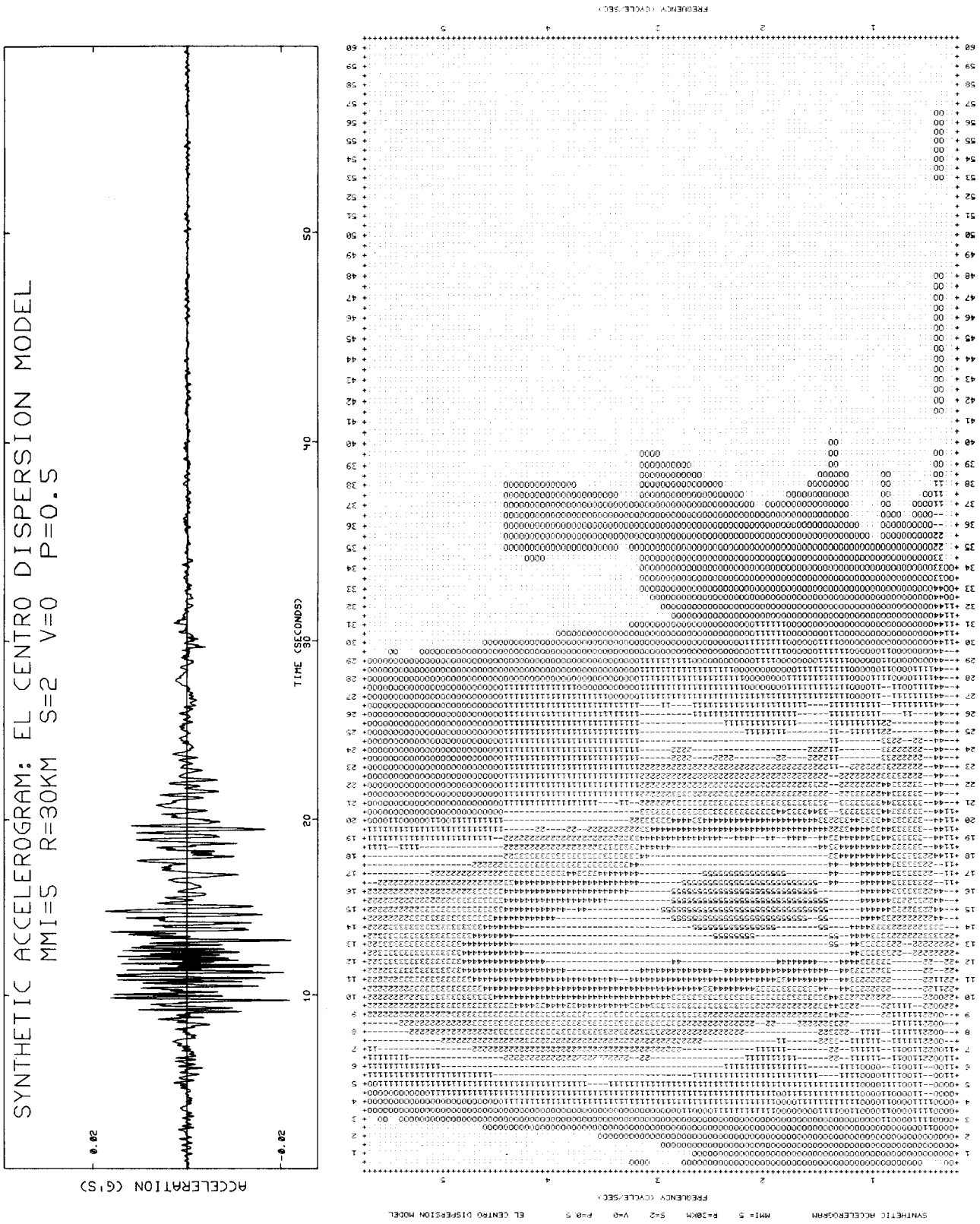
SYNTHETIC ACCELEROGRAM: EL CENTRO DISPERSION MODEL
MMI=5 R=30KM S=2 V=0 P=0.5
ACCELERATION (G'S)
0.02
-0.02
TIME (SECONDS)
10
20
30
40
50
FREQUENCY (CYCLE/SEC)
1
2
3
4
5

Figure 9

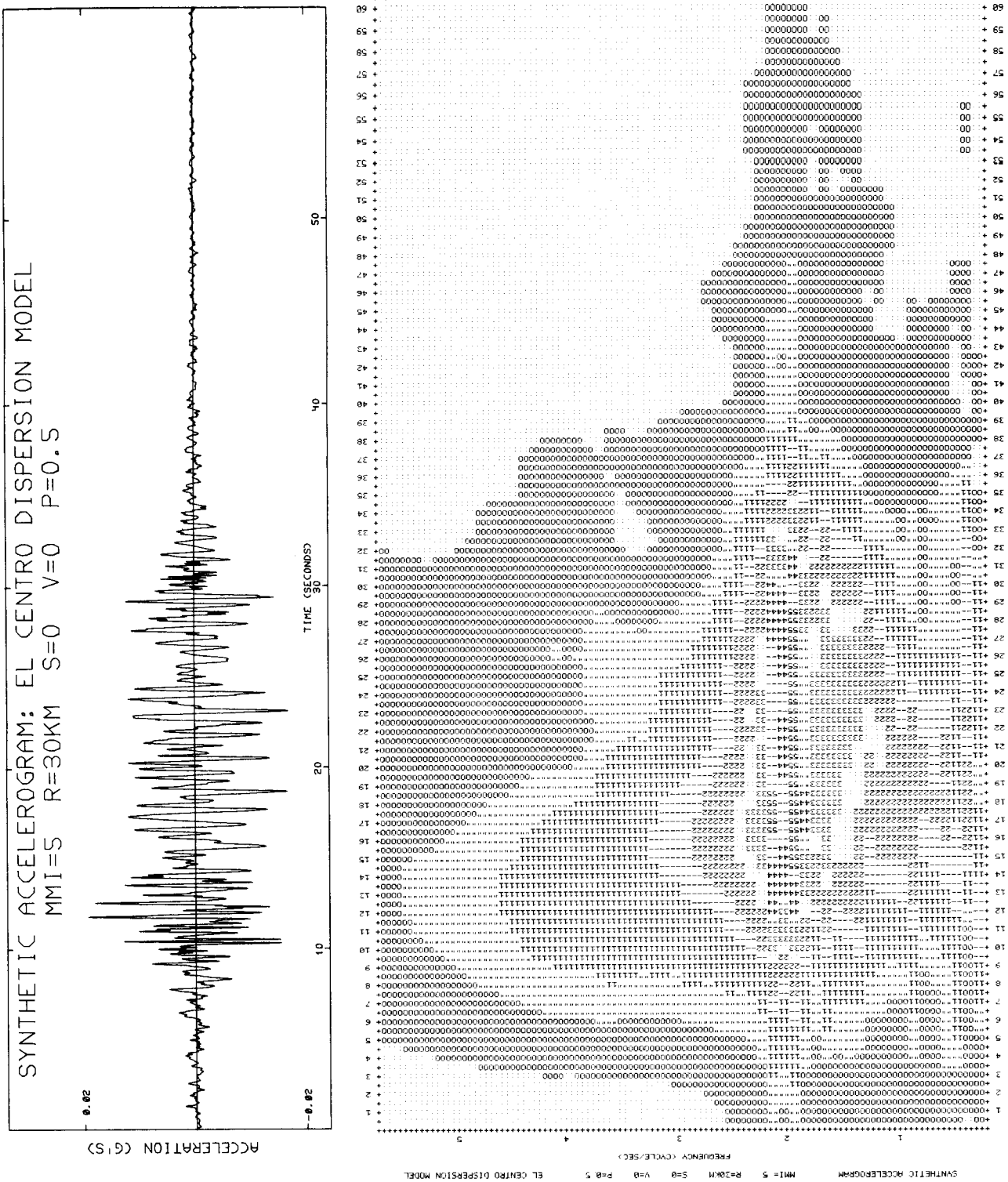
SYNTHETIC ACCELEROGRAM: EL CENTRO DISPERSION MODEL
MMI=5 R=30KM S=0 V=0 P=0.5
ACCELERATION (G'S)
TIME (SECONDS)
FREQUENCY (CYCLE/SEC)
SYNTHETIC ACCELEROGRAM MMI= 5 R=30KM S=0 V=0 P=0 5 EL CENTRO DISPERSION MODEL

Figure 10

Using these frequency bands, the correlation of duration with magnitude in each frequency band takes the form

$$D = as + bM + cR + d \pm \sigma \tag{18}$$

where s is the site classification parameter, M is the magnitude, R is the epicentral distance and σ is the standard deviation. It was found that the vertical and horizontal components of the accelerograms have to be analysed separately, so the coefficients a, b, c, d and σ are tabulated in Table V for both vertical and horizontal components. For cases where MMI is used, the available data are collected into the form of a table with the site condition and MMI as independent variables. The results are tabulated in Table VI.

EXAMPLES

Following the development in equations (8)–(13), and by employing equations (14)–(19), one can readily devise a computer program to calculate a synthetic accelerogram.[37]

Figures 3–6 present examples of artificial accelerograms computed for selected scaling parameters and using frequency-dependent duration. In addition to synthetic acceleration, these figures show the frequency- (cps) and time- (s) dependent amplitudes in equation (13) normalized so that the largest amplitude is equal to 5. To avoid cluttering and to show the significant contribution to synthesized acceleration, in these figures we present these amplitudes only for $f < 5{\cdot}75$ cps. All accelerograms were calculated, however, for $0{\cdot}07 \leqslant f \leqslant 25$ cps.

The effect of different site conditions ($s = 2$ for basement rock and $s = 0$ for alluvium) is shown in Figures 7 and 8 for $M = 6{\cdot}5$, $R = 20$ km, $v = 0$ and $p = 0{\cdot}5$. While the overall acceleration amplitudes are quite similar, for $s = 0$ duration of strong shaking is longer than for $s = 2$.

Figures 9 and 10 present a similar comparison between $s = 0$ and $s = 2$ (alluvium and basement rock sites) and for MMI = V, $R = 30$ km, $v = 0$ and $p = 0{\cdot}5$. Other examples of artificial accelerograms computed in terms of M and R or MMI and R have been presented by Wong and Trifunac.[37] They also show how equations (15) and (16) and the correlations of the duration of strong shaking can be refined to include the depth of sedimentary deposits beneath the station.

CONCLUSIONS

In this paper, we have presented a method for synthesizing realistic strong motion accelerograms for use in engineering design. The advantages of this method are that the results have almost all known characteristics of recorded strong shaking. In particular, these artificial accelerograms have non-stationary characteristics in time which are derived from known dispersive properties of earthquake waves guided through shallow low velocity layers of the earth's crust. These dispersive characteristics can be introduced directly as an input into the computer program and thus can portray directly the geologic environment of each specific site. Other scaling functionals required for synthesis of artificial accelerograms presented here are (i) the Fourier amplitude spectrum and (ii) the frequency-dependent duration of strong shaking. These two functionals can be estimated either in terms of empirical scaling relations developed in terms of earthquake magnitude[32, 34] or in terms of Modified Mercalli Intensity.[33, 35]

ACKNOWLEDGEMENTS

We thank John G. Anderson and Bruce D. Westermo for critical reading of the manuscript and for useful suggestions.

This work was supported by a contract from the United States Nuclear Regulatory Commission.

REFERENCES

1. J. G. Anderson and M. D. Trifunac, 'On uniform risk functionals which describe strong earthquake ground motion: definition, numerical, estimation and an application to the Fourier amplitude of acceleration, Dept. of Civil Engng, *Report No. CE77-02*, U.S.C., Los Angeles (1977).
2. M. Amin and A. H. Ang, 'A nonstationary stochastic model for strong motion earthquakes', *Structural Research Series No. 306*, Dept. of Civil Engng, University of Illinois (1966).

3. J. L. Bogdanoff, J. E. Goldberg and M. C. Bernard, 'Response of a simple structure to a random earthquake-like disturbance', *Bull. Seism. Soc. Am.* **51**, 293–310 (1961).
4. V. V. Bolotin, 'Statistical theory of aseismic design of structures', *Proc. 2nd Wld Conf. Earthq. Engng*, Japan, 1365–1374 (1960).
5. G. N. Bycroft, 'White-noise representation of earthquakes', *J. Eng. Mech. Div., ASCE*, **86**, No. EM2, 1–16 (1960).
6. C. A. Cornell, 'Stochastic process models in structural engineering', *Technical Report No. 34*, Dept. of Civil Engng, Stanford University (1964).
7. L. E. Goodman, E. Rosenblueth and N. M. Newmark, 'Aseismic design of firmly founded elastic structures', *Trans. ASCE*, **120**, 782–802 (1955).
8. H. Goto, K. Toki and T. Aiyoshi, 'Generation of artificial earthquakes on digital computer for aseismic design of structures', *Proc. Japan Earthq. Engng Symp.* 25–30 (1966).
9. H. Goto and H. Kameda, 'Statistical inference on future earthquake ground motion', *Proc. 4th Wld Conf. Earthq. Engng*, Santiago, Chile (1969).
10. H. Goto and K. Toki, 'Structural response to nonstationary random excitation', *Proc. 4th Wld Conf. Earthq. Engng*, Santiago, Chile (1969).
11. H. Honda, 'The mechanism of earthquakes', Geophysics Institute, Tohoku University, **9**, 1–46 (1957).
12. G. W. Housner, 'Characteristics of strong motion earthquakes', *Bull. Seism. Soc. Am.* **37**, 19–31 (1947).
13. G. W. Housner, 'Properties of strong ground motion earthquakes', *Bull. Seism. Soc. Am.* **45**, 187–218 (1955).
14. G. W. Housner and P. C. Jennings, 'Generation of artificial earthquakes', *J. Eng. Mech. Div., ASCE*, **90**, No. EM1, 113–150 (1964).
15. D. E. Hudson, 'Response spectrum techniques in engineering seismology', *Proc. 1st Wld Conf. Earthq. Engng*, Berkeley, California (1956).
16. D. E. Hudson, 'Strong motion earthquake accelerograms, index volume', *Earthq. Eng. Res. Lab. EERL 76–02*, Calif. Inst. of Tech., Pasadena (1976).
17. P. C. Jennings, G. W. Housner and N. C. Tsai, 'Simulated earthquake motions', Earthq. Eng. Res. Lab., Calif. Inst. of Tech., Pasadena (1968).
18. H. Kameda, 'Stochastic process models of strong earthquake motions for inelastic structural response', *U.S.–Southeast Symp. Engng for Natural Hazards Protection*, Manila (1977).
19. J. Penzien and S. C. Liu, 'Nondeterministic analysis of nonlinear structures subjected to earthquake excitations', *Proc. 4th Wld Conf. Earthq. Engng*, Santiago, Chile (1969).
20. O. A. Rascon and A. C. Cornell, 'A physically based model to simulate strong earthquake records on firm ground', *Proc. 4th Wld Conf. Earthq. Engng*, Santiago, Chile (1969).
21. C. F. Richter, *Elementary Seismology*, Freeman, San Francisco, 1958.
22. E. Rosenblueth, 'Some applications of probability theory on aseismic design', *Proc. 1st Wld Conf. Earthq. Engng*, Berkeley, California (1956).
23. E. Rosenblueth and J. I. Bustamante, 'Distribution of structural response to earthquakes', *J. Eng. Mech. Div., ASCE*, **88**, No. EM3, 75–106 (1962).
24. M. Shinozuka and Y. Sato, 'Simulation of nonstationary random processes', *J. Eng. Mech. Div., ASCE*, **93**, No. EM1, 11–40 (1967).
25. H. Tajimi, 'A statistical method of determining the maximum response of building structure during an earthquake', *Proc. 2nd Wld Conf. Earthq. Engng*, Japan (1960).
26. M. D. Trifunac, 'Response envelope spectrum and interpretation of strong earthquake ground motion', *Bull. Seism. Soc. Am.* **61**, 343–356 (1971).
27. M. D. Trifunac, 'A method for synthesizing realistic strong ground motion', *Bull. Seism. Soc. Am.* **61**, 1739–1753 (1971).
28. M. D. Trifunac and J. G. Anderson, 'Preliminary empirical models for scaling absolute acceleration spectra', Dept. of Civil Engng, *Report No. 77–03*, U.S.C., Los Angeles (1977).
29. M. D. Trifunac, 'Stress estimates for San Fernando, California, earthquake of 9 February 1971: main event and thirteen aftershocks', *Bull. Seism. Soc. Am.* **62**, 721–750 (1972).
30. M. D. Trifunac, 'Tectonic stress and source mechanism of the Imperial Valley, California, earthquake of 1940', *Bull. Seism. Soc. Am.* **62**, 1283–1302 (1972).
31. M. D. Trifunac, 'Analysis of strong earthquake ground motion for prediction of response spectra', *Earthqu. Eng. Struct. Dyn.* **2**, 59–69 (1973).
32. M. D. Trifunac, 'Preliminary empirical model for scaling Fourier amplitude spectra of strong ground acceleration in terms of earthquake, magnitude, source to station distance and recording site conditions', *Bull. Seism. Soc. Am.* **66**, 1343–1373 (1976).
33. M. D. Trifunac, 'Preliminary empirical model for scaling Fourier amplitude spectra of strong motion acceleration in terms of modified Mercalli intensity and geologic site conditions', *Earthqu. Eng. Struct. Dyn.*, **7**, 63–74 (1979).
34. M. D. Trifunac and B. D. Westermo, 'Dependence of duration of strong earthquake ground motion on magnitude, epicentral distance, geologic conditions at the recording station and frequency of motion', Dept. of Civil Engng, *Report No. 76–02*, U.S.C., Los Angeles (1976).
35. M. D. Trifunac and B. D. Westermo, 'Correlations of frequency dependent duration of strong earthquake ground motion with the modified Mercalli intensity and the geologic conditions at the recording stations', Dept. of Civil Engng, *Report No. 77–03*, U.S.C., Los Angeles (1976).
36. M. D. Trifunac and A. G. Brady, 'A study on the duration of strong earthquake ground motion', *Bull. Seism. Soc. Am.*, **65**, 581–626 (1975).
37. H. L. Wong and M. D. Trifunac, 'Synthesizing realistic strong motion accelerograms, Depart. of Civil Engng, *Report No. CE 78–07*, U.S.C., Los Angeles (1978).